1
Introduction

A variety of imaging techniques, first of all computed tomography, yield spatial (3D) images of micro-structures of materials on various scales as well as biological structures, food, snow and ice. This book is dedicated to methods for the quantitative analysis of the resulting 3D image data. Most of the described methods are rooted in discrete, differential, integral, and stochastic geometry, and mathematical morphology. The application examples focus attention on characterizing material structures, while the algorithms are of course of a general nature. A short and by no means complete overview of imaging techniques yielding spatial information is given below.

The number of methods for creating 3D image data as well as the number, quality, and content of the images is growing fast. While 512^3 pixels with 8 bit grey values were a large data set a couple of years ago, 2048^3 pixels with 16 bit grey values are the rule rather than the exception nowadays. Microcomputed tomography (μCT), as the most affordable 3D imaging technique, found its way into laboratories not only in research institutions but also in industry. The resulting wealth of 3D image data increases the need for efficient and objective analysis. The mere size of the images demands particularly fast algorithms and very careful memory management.

Contrary to classical materialography based on 2D images, using the full spatial information contained in 3D images allows, for example detailed directional analyses, estimation of particle-size distributions without shape assumptions, and judgement of the 3D connectivity of a structure, to name but a few. Moreover, macroscopic material properties can be simulated in the 3D images or in geometric models fit to the microstructure. The other side of the coin is the difficulty in visualizing and visually evaluating the results of processing or analysis steps. Special techniques for visualization – rendering, slicing, animation – are needed and visual assessment has generally to be distrusted.

We felt that this book was needed because a variety of image processing and analysis algorithms are a magnitude more complex than in 2D although in principle the algorithm works the same way. Perhaps the most striking example is the labelling of connected components. At first sight, this algorithm does not even seem to depend on dimension at all: a foreground pixel is given a label, all pixels connected to it are searched, found, and also labelled, then the next unlabelled foreground

3D Images of Materials Structures. Joachim Ohser and Katja Schladitz

ISBN: 978-3-527-31203-0

pixel is taken and so on. Looking closer one detects that even the deeper basis of this algorithm becomes unsafe when moving to dimensions 3 and higher. Classical concepts of discrete geometry like neighbourhood and complementarity do not transfer easily. Therefore, a significant part of this book is dedicated to building a sound basis for lattices, adjacency systems, complementarity, and connectivity.

In medical applications, 3D images have been processed and analyzed for much longer. However, the emphasis in medicine is often on making structures visible in the true sense of the word. The object of interest is known; manual interference is desired. Thus many problems discussed here, such as the equal treatment of different components or skeletonization exactly preserving the connectivity, play a minor role in medical image processing. On the other hand, we omit highly important issues such as registration and matching which certainly also play a role in materials science applications.

Time is not yet ripe for a standard reference on the analysis of 3D or multi-dimensional images of materials structures and this book does not intend to cover the topic comprehensively. The intention is rather to thoroughly explore some aspects of particular relevance for multi-dimensional image analysis, such as integral-geometric or spectral methods yielding efficient analysis algorithms. These penetrating, mathematically detailed key aspects are complemented by image processing and segmentation as well as simulation of macroscopic materials properties based on 3D image data from a practical applications point of view. More precisely, in Chapter 2, we introduce the notation and summarize the basics of image processing and analysis, which are used in the subsequent chapters. These are, in particular, the intrinsic volumes as basic characteristics, definition and characterization of random closed sets used for modelling components of microstructures, and some formulae from Fourier analysis helpful for definition and estimation of second-order properties. Image data are usually given on homogeneous lattices covered by Chapter 3. Connectivity of the lattice points is a crucial property, e. g. for surface rendering, labelling, watershed transform or skeletonization. We define connectivity using the concept of an adjacency system thus avoiding ambiguities in higher dimensions and we give an easy-to-check criterion for adjacency systems to be complementary. Chapter 3 also comprises a choice of segmentation and image-processing methods which, in our opinion, are particularly suited for the purpose of characterizing structures, more precisely microstructures, of materials: filters, morphological and distance transforms, labelling, and skeletonization.

The core of the book is Chapter 5 focusing on efficient measurement of characteristics by integrating the local information contained in 2^n pixel configurations, where n is the space dimension. Our method, based on integral geometry, takes up ideas from André Haas, Jean Serra, and Georges Matheron [109, 110, 323] and generalizes along essential lines to arbitrary dimensions. The resulting algorithms are fast and memory-saving and yield an amazing amount of structural information. The spectral analysis presented in Chapter 6 is closely related to diffraction experiments, well-established in material characterization. Diffraction by image processing is based on the Fourier transform, leading via the fast Fourier transform, to fast algorithms. Auto- and cross-covariance functions and their counterparts in the

inverse space (so-called Bartlett spectra) which are computed using the fast Fourier transform, are the natural quantities characterizing microstructural fluctuations. Moreover, spectral analysis does not rely on prior segmentation and therefore has potential for the analysis of low-contrast images. Stochastic geometric models for macroscopically homogeneous microstructures are covered in Chapter 7. Model fitting is illustrated for fibre and cellular structures on a few examples. Finally, Chapter 8 builds the bridge to the vivid and, in modern materials research, central topic of investigating the relations between microstructure and material properties. Here, this important issue can only be touched on. However, it is natural to use 3D image data as a starting point for finite-element methods. In particular, combined with the stochastic models from Chapter 7, this opens new opportunities in materials design and optimization. We clarify the simulation of macroscopic properties using the example of computation of mechanical properties of porous media based on 3D images obtained by microcomputed tomography.

This book incorporates ideas from many sources, first the various fields of geometry mentioned above, but also computer science, materials science, and physics as well as the list of reference documents. A small number of books which are particularly important to us will be listed here. Jean Serra's book [323] is a treasure trove for both mathematical morphology and stochastic geometry. Methods from integral and stochastic geometry play a central role in our understanding of image analysis. The standard reference is still the book [343] by Dietrich Stoyan, Wilfried Kendall, and Joseph Mecke which sets an example in uniting theory and application. Sound theoretical background on convex, integral, and stochastic geometry are provided by Rolf Schneider's and Rolf Schneider's and Wolfgang Weil's books [315, 317]. Not least, we have learned a lot from Gabriele Lohmann's pioneering book on 3D image processing [207].

While finalizing this book we came to know the recent book on 3D image processing by Junichiro Toriwaki and Hiroyuki Yoshida [360]. There are some striking parallel developments, however, in general the focus is rather on those subjects which are kept short in our book. This is not the least due to their motivation stemming from medical applications.

Image Sources

The term *tomography* summarizes imaging methods which deliver 3D data sets consisting of cross-sectional slices from the investigated sample. John Banhart [24] classifies tomographic techniques as

- **non-destructive, using projections only** like µCT,
- **non-destructive, using information beyond projection images** such as 3D X-ray diffraction [24, Chapter 9], and
- **destructive** such as position-sensitive ion microscopy – 3D atom probe [40].

Tomography in the strict sense denotes non-destructive methods reconstructing the 3D image data from projection images using *tomographic reconstruction*, only,

see [24, Chapter 2] for an overview and further references. Most data sets used in this book are acquired by X-ray computed tomography, which nowadays certainly accounts for the vast majority of 3D images of materials structures. Nevertheless there are several other 3D imaging techniques with particular potential for materials science applications briefly mentioned below, e. g. electron tomography or scanning electron microscopy combined with focused ion-beam thinning.
The idea of computed X-ray tomography dating back to [61] is to combine radiographic projection images of the linear X-ray attenuation coefficient from a set of different projection angles in order to reconstruct the mass distribution within a sample. Godfrey Hounsfield [139] transfered this idea into a device which imaged, non-destructively, parts of a body in three dimensions – the first tomograph. Computed tomography had a strong impact on medicine [140] and was quickly introduced into material science as well [281], where the resolutions reached the micrometer-scale (microtomography [91]).

Synchrotron radiation delivers images with low noise level and high contrast, due to the high available flux allowing short exposure times and mono-chromatization, as well as the nearly parallel beam eliminating cone-beam and fan-beam reconstruction artifacts. For the reconstruction of the tomographic images the filtered back-projection algorithm is commonly used [157]. Synchrotron radiation also allows one to use contrast mechanisms other than the classical X-ray attenuation:

- local electron density (phase contrast, holotomography) [59],
- chemical species distribution (fluorescence tomography) [329],
- inner surfaces and interfaces (refraction-enhanced tomography) [235],
- or local crystalline lattice quality (topo-tomography) [210].

For a comprehensive and recent overview of tomographic imaging techniques, see the compilation [24] edited by John Banhart. Examples of µCT images from both synchrotron and laboratory sources are abundant throughout the book. Sources of sample and image are usually given in the respective captions, except for the following frequent image sources which are given here in full, in order to keep the captions short.

- Fraunhofer Institut für Zerstörungsfreie Prüfung, (IZFP), Saarbrücken, Germany.
- Alexander Rack, now affiliated to the European Synchrotron Radiation Facility (ESRF, beamline ID22), Grenoble, France; formerly at Helmholtz-Zentrum Berlin, images taken at BAMline of Bessy (Berliner Elektronenspeicherring – Gesellschaft für Synchrotronstrahlung m.b.H.), ANKA (Forschungszentrum Karlsruhe, Institute for Synchrotron Radiation), and beamline ID22 at ESRF.
- Bernhard Heneka, RJL Micro&Analytic GmbH, Karlsdorf, Germany, images taken with various µCT-devices by SkyScan, Kontich Belgium.
- Lukas Helfen, affiliated to ANKA, imaging at beamline ID19 of ESRF.

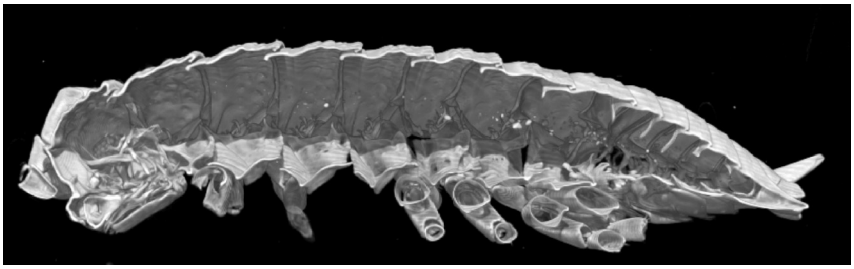

Fig. 1.1 The mineralized exoskeleton of the common woodlouse *Porcellio scaber*. The image was taken by µCT using synchrotron radiation (SRµCT scan, pixel spacing 11.35 µm) by F. Neues, Momentive Performance Materials GmbH, Leverkusen. The cuticle consists of calcium carbonate and chitin. A virtual cut was performed to create this picture. Sample provided by M. Epple, Universität Duisburg-Essen, Institut für Anorganische Chemie. Specimen by A. Ziegler, Universität Ulm. Total length of the animal is 8 mm. Visualization by VG Studio MAX.

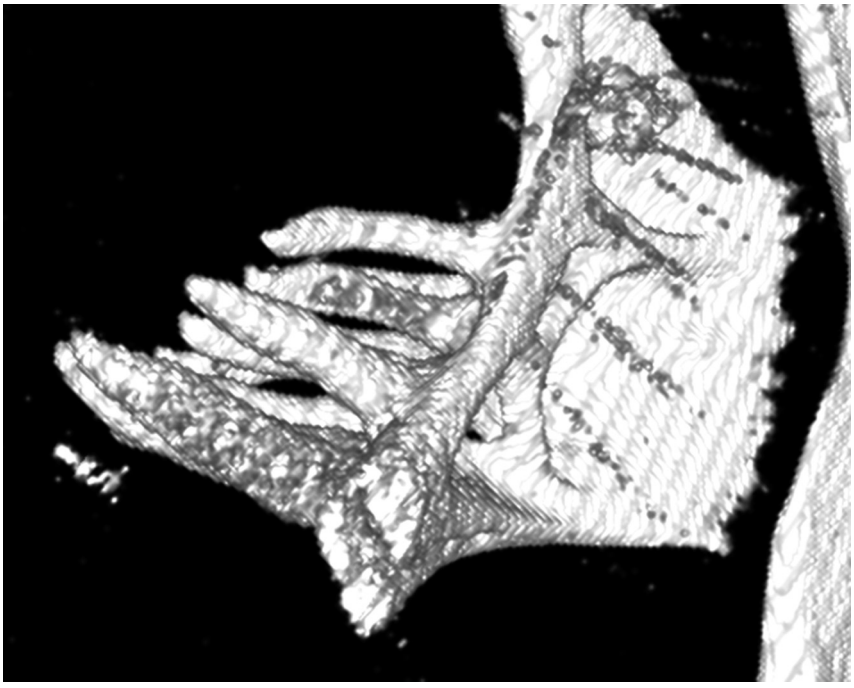

Fig. 1.2 SRµCT scan by F. Neues, Momentive Performance Materials GmbH, Leverkusen, of a branchial bone with the pharyngeal teeth of *Danio rerio* (pixel spacing 6.88 µm, length of a tooth approximately 0.2 mm). The teeth in *D. rerio* are replaced during the whole lifespan of the fish. Sample by W. Arnold, Universität Witten/Herdecke, image provided by M. Epple, Universität Duisburg-Essen, Institut für Anorganische Chemie. Visualization by VG Studio MAX.

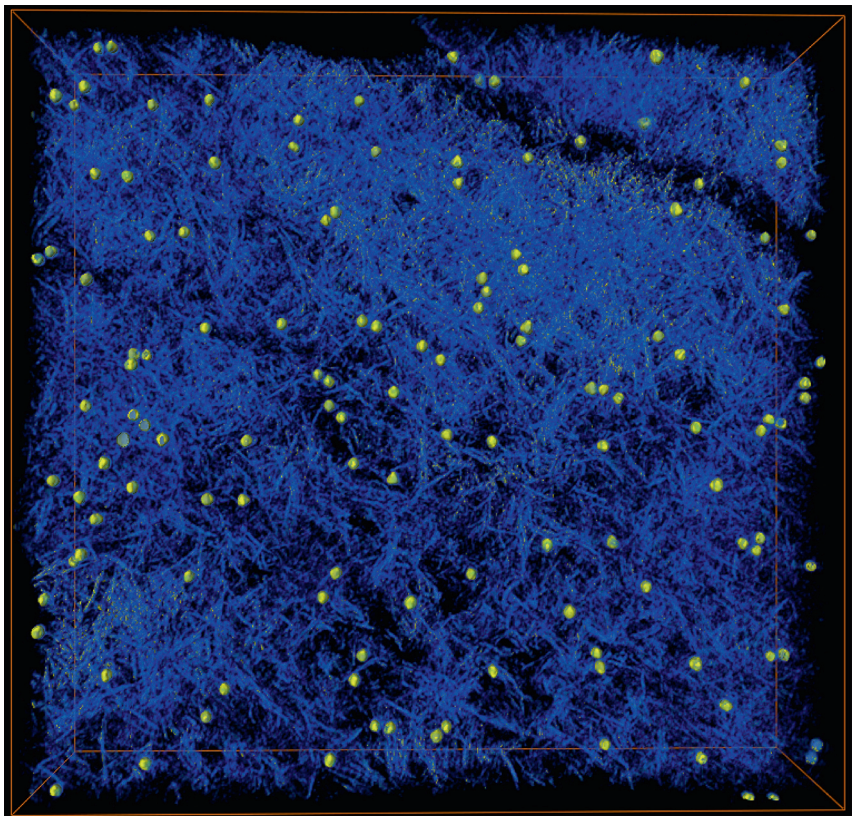

(a)

(b)

Fig. 1.3 Electron tomographic image of a catalyst produced by Haldor Topsoe for oil refining. Alumina support structure (4–5 nm thick) and 10-nm gold markers used for alignment, pixel spacing 0.69 nm. Images taken by C. Kübel, FEI Company, Eindhoven [181]. Visualizations made using Amira. (a) Volume rendering of $700 \times 700 \times 150\,\mathrm{nm}^3$. (b) Surface rendering of a sub-volume of approx. 100 nm edge length revealing the sheet-like structure of the support material.

Images of biological objects scanned at Hamburger Synchrotronstrahlungslabor (HASYLAB) of Deutsches Elektronen-Synchrotron (DESY) are shown in Figures 1.1 and 1.2. For details about the aims of the investigation see [242, 243].
Another tomographic technique is *electron tomography*. Here a series of 2D projection images obtained by (scanning) transmission electron microscopy ((S)TEM) of the tilted sample at angles in the range $[-75°, 75°]$ or $[-65°, 65°]$ are reconstructed into a 3D image. The projection images are taken either in bright field TEM mode or high-angle angular dark field STEM mode where the latter also allows imaging of crystalline structures. Resolution depends strongly on the nature and thickness of the sample as well as the maximal tilt angle, but can reach 1 nm. An example is shown in Figure 1.3. The book [24] also includes a chapter on electron tomography.

There are various further 3D imaging techniques. One of these is scanning electron microscopy (SEM) combined with focused ion beam (FIB) thinning. Depending on the lateral resolution of SEM and the thinning rate of FIB, a pixel spacing down to 10 nm can be achieved [134, 367]. As an example we show the lamellar structure of cast iron with flake graphite, see Figure 1.4. SEM with FIB is in princi-

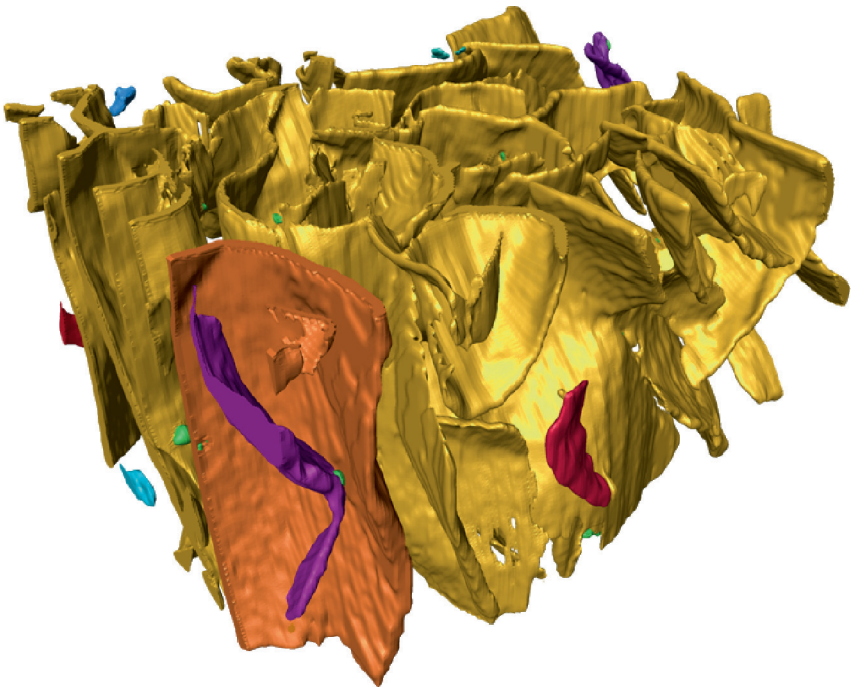

Fig. 1.4 Flake graphite in cast iron. The image was taken by scanning electron microscopy (SEM) combined with focused ion beam (FIB) thinning of the corresponding cast iron specimen. Sample by Halberg Guss GmbH, imaging by A. Velichko, Universität des Saarlandes, Institut für Funktionswerkstoffe. Visualization using Amira. Visualized are $460 \times 275 \times 200$ which correspond at pixel spacings of $0.185\,\mu m \times 0.235\,\mu m \times 0.5\,\mu m$ to $85.1\,\mu m \times 64.6\,\mu m \times 100\,\mu m$ [367].

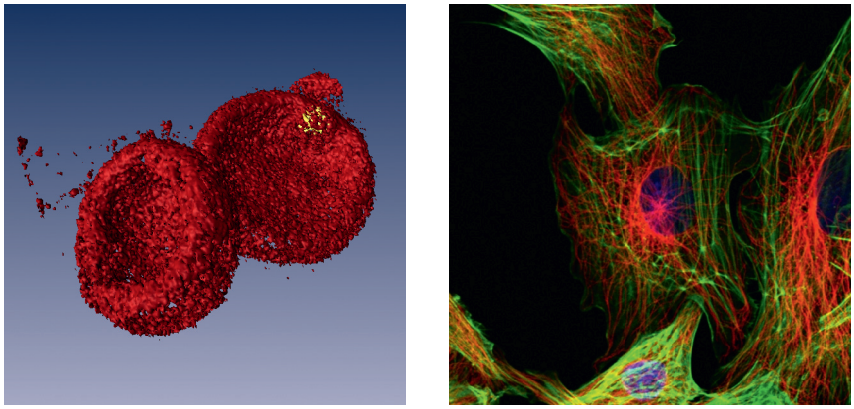

(a) (b)

Fig. 1.5 Images taken by CLSM using a 4 Pi microscope of Leica, glycerol 100×/1.35 corr objective. Shown are 512 × 512 × 20 pixels. (a) Two human red cells, one infected by malaria (yellow pixels), image taken by J.A. Dvořak and F. Tokumasu, National Institute of Allergy and Infectious Diseases, NIH, Washington, surface rendering using Amira, uniform pixel spacing of 30 nm. (b) Snap fibres of a mouse cell, blue: kernel coloured with DAPI, red: cytoskeleton protein coloured with Vimentin, green: cytoskeleton protein coloured with Tubulin. Image taken by T. Szellas, Leica Microsystems CMS GmbH, Mannheim, specimen provided by G. Giese, Max Planck Institute for Medical Research, Heidelberg, volume rendering using Leica LCS, pixel spacings 30 nm, 30 nm and 100 nm.

ple a serial sections technique which does not include tomographic reconstruction. Nevertheless, it is said to be *focused ion beam nanotomography*.

Figures 1.5 and 1.6 show 3D images obtained by confocal laser scanning microscopy (CLSM) and fluorescence microscopy, respectively. The generation of 3D data by CLSM often needs a correction for the light attenuation, while fluorescence images are improved by certain deconvolution techniques, see, e. g. [307] where a generalized approach for an accelerated, maximum likelihood-based image restoration is suggested.

If not otherwise mentioned, all 3D renderings, image processing, and analysis examples are made with MAVI or MAVIlib, respectively, created at the Fraunhofer-Institut für Techno- und Wirtschaftsmathematik (ITWM) in Kaiserslautern [94]. MAVI's roots are Joachim Ohser's library of C algorithms for stochastic geometry, stereology, spatial statistics applied to images of materials microstructures and a three-year 3D image analysis project funded by the research foundation of Rheinland-Pfalz which started in 1999. Over the course of nearly ten years MAVI has constantly grown by incorporating algorithms developed at Fraunhofer ITWM as well as implementations of algorithms that proved to be successful and of general interest in a variety of projects. MAVI's current software design is due to Michael Godehardt and Björn Wagner and inspired by the generic programming setup of Ulrich Köthe's VIGRA C++-library [176, 177].

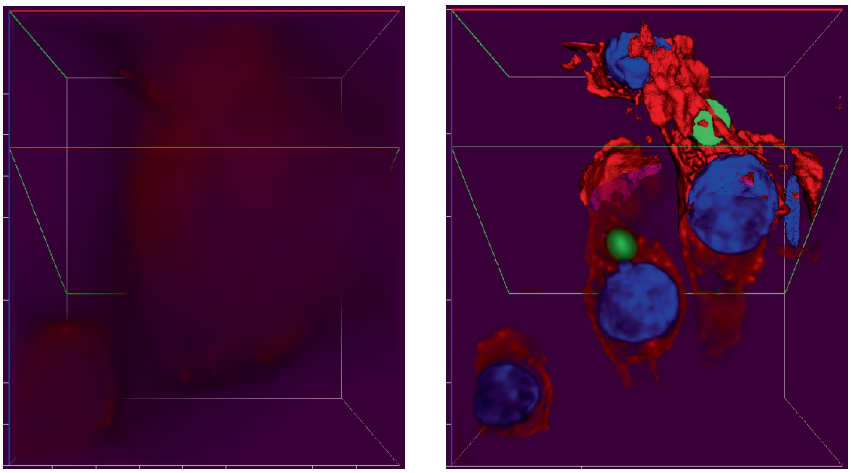

(a) (b)

Fig. 1.6 Fluorescent 3 channel 3D image of a Zymosan treated mouse macrophage cell line taken with a Carl Zeiss fluorescence research microscope Axiovert 200 M equipped with a Plan APOCHROMAT 63×/1.4 NA objective and an AxioCam HRm cooled CCD camera. Image provided by B. Kraus, Pharmazeutische Biologie, Universität Regensburg. Red: f-actrin coloured with phalloidine rhodamine. Blue: kernels, coloured with Hoechst 33342. Green: Zymosan yeast cell walls, coloured with Bodipy-FL, 432 × 504 × 111 pixels, pixel spacings (106, 106, 280) nm. Because of an oversampling in the xy-plane by a factor of about 2.5, it is possible to deconvolve the original image using an iterative, regularized and accelerated maximum-likelihood algorithm resulting in a considerably improved resolution and contrast in the widefield image. (a) Original image. (b) Widefield image.

We do not intend to give a complete overview of 3D image processing software in the following. However, we give a short and subjective choice of tools which we find useful at least for some tasks. There is a wide range of high-quality visualization tools also offering 3D processing algorithms, some of which are very sophisticated and, to a more limited extent, characterization. Examples are the widely used commercial software systems VGStudio MAX by Volume Graphics and Amira/Avizo by Mercury Systems. Visualizations made with these two systems are also featured in this book. Advanced Visual Systems offers with AVS/Express a powerful tool box for visualization. For research purposes vtk/itk (www.itk.org, C++) and ImageJ (rsb.info.nih.gov/ij, Java) offer open source libraries focused on medical image segmentation and processing and microscopy data, respectively. DIPlib (www.diplib.org, C, MATLAB interface) can be used non-commercially under a free licence. IDL (Interactive Data Language) by ITT Visual Information Solutions is a commercial high-level programming language offering a wide variety of image processing algorithms and thus allowing fast creation of user-defined applications.